The class III ribonucleotide reductase from *Neisseria bacilliformis* can utilize thioredoxin as a reductant

Yifeng Wei[a,1], Michael A. Funk[a], Leonardo A. Rosado[a], Jiyeon Baek[a], Catherine L. Drennan[a,b,c,1], and JoAnne Stubbe[a,b,1]

Departments of [a]Chemistry and [b]Biology, and [c]Howard Hughes Medical Institute, Massachusetts Institute of Technology, Cambridge, MA 02139

Contributed by JoAnne Stubbe, July 29, 2014 (sent for review July 13, 2014)

The class III anaerobic ribonucleotide reductases (RNRs) studied to date couple the reduction of ribonucleotides to deoxynucleotides with the oxidation of formate to CO_2. Here we report the cloning and heterologous expression of the *Neisseria bacilliformis* class III RNR and show that it can catalyze nucleotide reduction using the ubiquitous thioredoxin/thioredoxin reductase/NADPH system. We present a structural model based on a crystal structure of the homologous *Thermotoga maritima* class III RNR, showing its architecture and the position of conserved residues in the active site. Phylogenetic studies suggest that this form of class III RNR is present in bacteria and archaea that carry out diverse types of anaerobic metabolism.

The class III ribonucleotide reductases (RNRs) are glycyl radical enzymes present in many strict and facultative anaerobes that catalyze the conversion of nucleotides to deoxynucleotides (1, 2) via a mechanism involving complex free radical chemistry and are largely responsible for providing the balanced pool of deoxynucleotides required for DNA synthesis and repair (3). The class III RNRs that have been characterized thus far obtain the reducing equivalents required to make deoxynucleoside triphosphates (dNTPs) from the oxidation of formate to CO_2 (4). Here we report a second subtype of class III RNR from *Neisseria bacilliformis*, which can obtain its reducing equivalents from the thioredoxin (TrxA)/thioredoxin reductase (TrxB)/NADPH system.

RNRs provide the only pathway for de novo biosynthesis of dNTPs (5). They share a structurally homologous active site architecture in the α subunit and a partially conserved, radical-based reduction mechanism. RNRs have been isolated and characterized from all kingdoms of life and, based on the characterization of these proteins thus far, are divided into three classes (I, II, and III) according to the metallo-cofactor used to generate a thiyl radical that initiates the radical-dependent reduction chemistry (6). The class I RNRs use cofactors generated by the reaction of reduced metals (Fe, Mn, and Fe/Mn) and O_2 and are present only in aerobic organisms. The class II RNRs use adenosylcobalamin in an O_2-independent reaction and are present in both aerobes and anaerobes. The class III RNR uses an O_2-sensitive glycyl radical (G•) (2) situated in the α protein (NrdD), which is generated by a separate activating enzyme (NrdG) via radical *S*-adenosylmethionine (SAM)-$[4Fe4S]^{1+}$ chemistry (7, 8). The class III RNRs are only found in facultative and obligate anaerobes. A second distinction between the three classes has been the source of the reducing equivalents for nucleotide reduction. In the class I and II RNRs, they are provided by a redoxin (thioredoxin, glutaredoxin, or NrdH), which is rereduced by thioredoxin reductase and NADPH (9–11). In contrast, for the bacteriophage T4 (12), its Gram-negative host *Escherichia coli* (1), and the Gram-positive *Lactococcus lactis* (13), the only class III RNRs characterized in detail to date, nucleotide reduction is coupled to the oxidation of formate to CO_2 (4).

Formate in *E. coli* and *L. lactis* is provided by carrying out the fermentation of sugars to acetate and formate via a pathway involving pyruvate-formate lyase (PFL) (14, 15). For *E. coli* growing in the absence of electron acceptors, formate induces the formate-hydrogenlyase pathway in which it is converted to the waste products H_2 and CO_2 by formate dehydrogenase (FDH) and hydrogenase (16). However, there are many proteins annotated as class III RNRs present in diverse bacteria and archaea (17, 18) which do not possess PFL or generate formate as an intermediate or end product in their primary metabolism (19), suggesting that an alternative reducing system for class III RNRs might be involved. This variability in the presence of formate-producing pathways is in contrast to the ubiquitous distribution of thioredoxin-like proteins used by the class I and II RNRs. This observation prompted us to carry out a bioinformatics search for candidate class III RNRs that use disulfide chemistry similar to the class I and II enzymes.

The generic mechanism of nucleotide reduction by all three classes of RNRs can be divided into two half reactions: the radical initiation process and the reduction process (Fig. 1) (20, 21). In all RNR classes, nucleotide reduction is initiated by generating a 3′-nucleotide radical (22–24) (Fig. 1*A*, **2**) via a transient, conserved, top face thiyl radical (25) (**1**) on the Cys loop in the active-site. This reaction likely involves general base catalysis by a conserved glutamate (class I and II RNRs), and perhaps formate (class III RNRs) (26), which facilitates loss of water to form a ketyl radical (**3**). In the class I and II RNRs, reduction of the ketyl radical to a 3′-keto-deoxynucleotide intermediate is accompanied by the oxidation of the conserved cysteines (27) on the bottom face of the nucleotide to a disulfide anion radical (28) (Fig. 1*B*, **4**), which serves as the reductant for the ketonucleotide, forming a 3′-deoxynucleotide radical and a disulfide (**5**). Product formation is accompanied by regeneration of the top face thiyl radical (**6**). Rereduction of the active-site disulfide by thioredoxin

Significance

Ribonucleotide reductases (RNRs) catalyze nucleotide reduction via complex radical chemistry, providing deoxynucleotides for DNA synthesis in all domains of life. Many anaerobic bacteria and archaea contain the class III O_2-sensitive RNR, and those that have been studied to date couple nucleotide reduction to formate oxidation. Here we report the characterization of a second class III RNR subtype that couples nucleotide reduction to the oxidation of thioredoxin. Because of the central role of formate and thiols in many anaerobic processes, the distribution of class III RNRs among different organisms may shed light on aspects of anaerobic biochemistry.

Author contributions: Y.W., M.A.F., L.A.R., C.L.D., and J.S. designed research; Y.W., M.A.F., L.A.R., and J.B. performed research; and Y.W., M.A.F., L.A.R., C.L.D., and J.S. wrote the paper.

The authors declare no conflict of interest.

Data deposition: The atomic coordinates and structure factors have been deposited in the Protein Data Bank, www.pdb.org (PDB ID code 4U3E).

[1]To whom correspondence may be addressed. Email: yifwei@mit.edu, cdrennan@mit.edu, or stubbe@mit.edu.

This article contains supporting information online at www.pnas.org/lookup/suppl/doi:10.1073/pnas.1414396111/-/DCSupplemental.

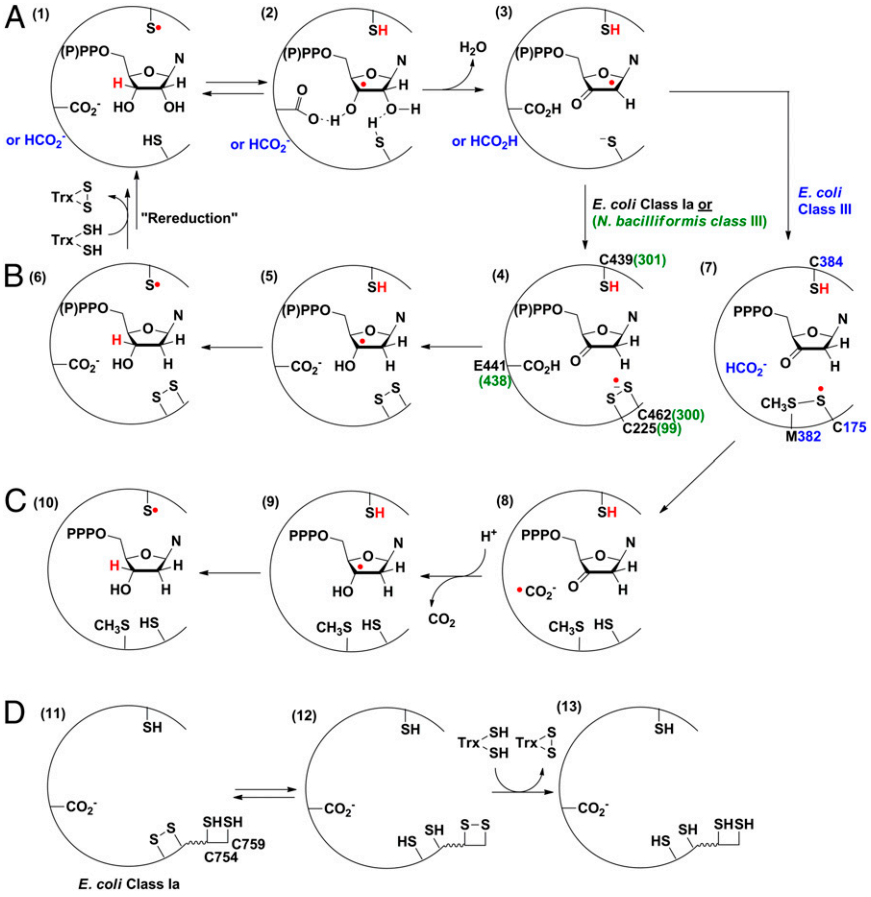

Fig. 1. Mechanistic model for nucleotide reduction by RNRs. (*A*) First half reaction common to all RNRs. (*B*) Second half reaction of *E. coli* class Ia and *N. bacilliformis* class III RNR. (*C*) Second half reaction of *E. coli* class III RNR. M382 in *E. coli* class III RNR is located two residues from the top face thiyl radical (C384), in a position similar to the conserved N437 in *E. coli* class Ia RNR, which makes a hydrogen bond to the 2′-OH group of the substrate. (*D*) Mechanistic model for rereduction of the active site disulfide in class I and II RNRs via a pair of conserved cysteines on the C-terminal tail of α.

occurs via disulfide exchange with a pair of conserved cysteines on the C-terminal tail of α (Fig. 1*D*) (27).

In the class III RNR, only one of the disulfide-forming cysteines in the active site is conserved (21, 29, 30), and we recently showed (31) that reduction of the ketyl radical to the 3′-keto-deoxynucleotide is accompanied by the formation of a thiosulfuranyl radical (Fig. 1*C*, **7**) between the bottom face cysteine thiyl radical and a methionine residue. The thiosulfuranyl radical, in equilibrium with the thiyl radical, then oxidizes formate to a $\bullet CO_2^-$ radical (21) (**8**), proposed to serve as the reductant for the 3′-keto-deoxynucleotide. In all classes, the 3′-keto-deoxynucleotide intermediate (Fig. 1 *B*, **4**, or *C*, **7**) is proposed to be reduced by proton-coupled electron transfer (32), with the source of the proton being the conserved glutamate in the class I and II RNRs, and unknown in the class III RNR.

Because of the role of this methionine residue in the reaction with formate in the *E. coli* class III RNR, we expected that it would be conserved in all formate-dependent NrdDs. However, just as the pathways for formate production are not conserved, our search in the RNRdb (33) showed that this methionine is missing in a set of NrdD sequences. In addition, all annotated NrdD sequences lacking this methionine residue invariably contain an additional cysteine residue immediately preceding the conserved thiyl radical on the Cys loop. This location may allow formation of a disulfide between the additional cysteine and the conserved bottom face thiol, thus allowing the reducing equivalents to be provided by chemistry similar to that in the class I and II RNRs.

To establish whether some class III RNRs use a formate-independent reduction strategy, a number of candidate class III RNRs were cloned and expressed. We now report the characterization of the NrdD and NrdG proteins from *Neisseria bacilliformis* (NbNrdD and NbNrdG) (34, 35). This organism lacks the fermentative pathway terminating in PFL, a major source of formate for the class III RNRs studied to date, and its NrdD lacks the active site methionine. In addition, we were able to clone, express, isolate, and crystallize a related NrdD from the deep-branching thermophilic bacterium *Thermotoga maritima* (TmNrdD, 30% sequence identity with NbNrdD; Fig. S1). The mesophilic NbNrdD proved more amenable to biochemical studies, and we demonstate that it is a G• enzyme and show that, like the previously characterized class III RNRs, NTPs are substrates. We also show that formate is unable to provide the reducing equivalents to make dNTPs. This organism possesses a TrxA that has 61% sequence identity with *E. coli* TrxA, and activity can be reconstituted in vitro using the *E. coli* TrxA/TrxB/NADPH system. The X-ray structure of TmNrdD reported here provides our framework for modeling the conserved residues in this newly discovered class III RNR subtype and supports the hypothesis for the NbNrdD that three cysteines and a glutamate are located in the active site region where they can play a role in catalysis. The distribution and significance of this form of class III RNR are discussed.

Results

Our bioinformatics analysis, leading to the identification of a previously unidentified class III RNR subtype that couples nucleotide

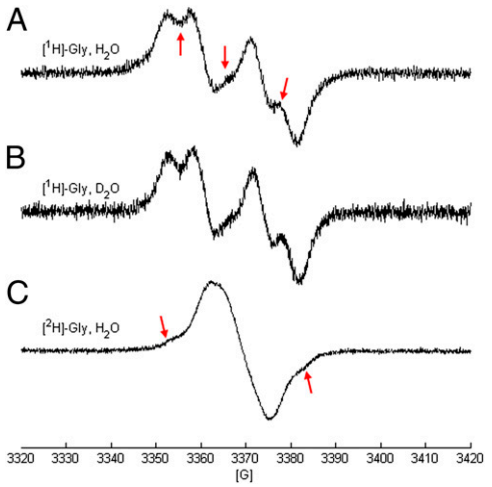

Fig. 2. X-band EPR spectra of the NbNrdD G•. (*A*) NbNrdD in H_2O, arrows indicate features arising from hyperfine coupling to nonexchangeable protons. (*B*) NbNrdD in D_2O. (*C*) [^{2}H]-Gly-NbNrdD in H_2O. Arrows indicate features possibly due to contaminating unlabeled NbNrdD.

reduction to disulfide bond formation, is described below. To test our hypothesis, we attempted to clone, express, and purify six of the class III RNRs of this subtype, including the enzymes from *N. bacilliformis*, *T. maritima*, *Shewanella sediminis*, *Pyrococcus furiosus*, *Pseudomonas aeruginosa*, and *Schizosaccharomyces japonicas*. The NbNrdD and NbNrdG were soluble and could be obtained in reasonable amounts and thus became the focus of our attention.

NbNrdD Is a G• Enzyme. To generate active NbNrdD for biochemical studies, we incubated NbNrdD with NbNrdG and SAM in the presence of the acriflavin/bicine photoreduction system (31), resulting in the generation of a radical with an electron paramagnetic resonance (EPR) signal shown in Fig. 2*A*. The spectrum reveals a dominant hyperfine coupling constant of 40 MHz, proposed to be associated with the H_α of glycine, consistent with its assignment as G•. Uniform labeling of NrdD with [^{2}H]-glycine resulted in the collapse of the signal into a singlet (Fig. 2*C*), establishing the assignment. Additional spectral features (indicated with arrows in Fig. 2*A*), which persist even when the activation reaction is carried out in D_2O (Fig. 2*B*), are also visible for the PFL G•, although less well resolved (36). These features are attributed to hyperfine coupling with additional nonexchangeable protons, likely the α-protons of the two adjacent amino acids in the sequence (36). These interactions are predicted to be affected by the conformation of the peptide backbone, leading to variations in the G• EPR spectra between different G• enzymes. The lack of exchange of the H_α of glycine with D_2O, previously shown to occur with PFL (37), is similar to observations for the G• of *E. coli* class III RNR (38).

NbNrdD Catalyzes CTP Reduction Using TrxA/TrxB/NADPH. Our hypothesis is that reducing equivalents for nucleotide reduction by NbNrdD are delivered by a redoxin, similar to the class I and II RNRs (Fig. 1 *A* and *B*). To identify a candidate redoxin for NbNrdD, we first carried out a BLAST search using the NbNrdD sequence. This search yielded a set of related sequences with ∼50% pairwise identity in diverse organisms, including *Shewanella sediminis* (gammaproteobacterium), *Bacteroides ovatus* (Sphingobacteria), and *Clostridium citroniae* (Firmicutes). Examination of the redoxins present in these organisms revealed that only TrxA/TrxB is conserved. The high sequence identity between *N. bacilliformis* TrxA and *E. coli* TrxA (61% identity; Fig. S2), which has been used in assays for other class I and II RNRs (39–41), suggested that *E. coli* TrxA could be used in our activity assays.

The assays were thus carried out with NbNrdD (0.25 G•/α) and *E. coli* TrxA/TrxB/NADPH, and the results are summarized in Table 1. NbNrdD was active for reduction of CTP to dCTP with ATP as an effector, but nearly inactive for CDP reduction (∼3% of the activity for CTP reduction; Table 1). Catalytic activity was dependent on the presence of G• and TrxA (Table 1). Formate failed to produce any dCTP. Unexpectedly the activity was the same in the absence or presence of allosteric effectors (ATP or dATP; Table 1). NbNrdD lacks the ATP cone domain that controls the activity of many RNRs by binding the activator (ATP) or the inactivator (dATP) (42). Thus, in NbNrdD, both ATP and dATP would be predicted to bind to the specificity site and activate nucleotide reduction. The activity that we have obtained with NbNrdD is ∼0.24 s^{-1} per G•, which is 20-fold lower than that of *E. coli* NrdD, which is ∼4 s^{-1} per G• (43). We hypothesize that the low activity and insensitivity to allosteric effectors is a result of *E. coli* TrxA functioning as a suboptimal reductant, making rereduction of the active site disulfide, rather than nucleotide reduction, rate limiting (44). Further study of the allosteric regulation of this enzyme will likely be facilitated by cloning, expressing, and using the *N. bacilliformis* Trx system in our assays.

The number of dCTPs formed per NADPH in the reaction mixture is 0.97 (Fig. 3), suggesting a 1:1 stoichiometry, in agreement with the proposal that the reducing equivalents are provided by the TrxA/TrxB/NADPH system (Fig. 1 *A* and *B*). The ∼26 turnovers per G• that occur without addition of NADPH are attributed to the reduction of TrxA by residual DTT carried over from the NbNrdD storage buffer (∼27 μM), which is essential for maintaining enzymatic activity.

NbNrdD(C301A) Is Inactive, and Reaction of NbNrdD(C300A) with CTP Generates Cytosine (Cyt). To test our hypothesis that C301 forms the top face thiyl radical that initiates nucleotide reduction (Fig. 1 *A* and *B*), the NbNrdD(C301A) mutant was generated. This mutant is inactive in dCTP and Cyt formation, despite having 0.25 G•/α2, consistent with our model. We propose that C300 in NbNrdD, which is adjacent to the top face thiyl radical residue C301 on the Cys loop (Fig. 1*B* and Fig. 6*A*), plays a role analogous to that of C462 in the *E. coli* class Ia α protein (NrdA) (Fig. 1*B*), donating reducing equivalents for nucleotide reduction by generating a disulfide with C99 (Fig. 1*B*). To test this hypothesis, we generated the NbNrdD(C300A) mutant and reacted it with CTP. The analogous C462A mutation in *E. coli* NrdA results in the generation of a 3′-keto-deoxycytidine intermediate (Fig. 4*B*, **16**) that decomposes to release Cyt (**17**) (27).

The G• of the NbNrdD(C300A) has an EPR spectrum identical to that of the WT-NbNrdD and is generated with a similar efficiency. Reaction of NbNrdD(C300A) with 5-[^{3}H]-CTP leads to the time-dependent release of ∼5.5 equivalents of 5-[^{3}H]-Cyt per G• (Fig. 4*A*), identified by HPLC (Fig. S3), with an initial rate of

Table 1. Requirements for dCTP formation by NbNrdD

Reaction conditions	Activity (U/mg)
Complete (CTP, ATP)	49
−SAM (no G• formed)	ND
−TrxA	ND
−TrxA, + formate (10 mM)	ND
−ATP	47
−ATP, +dATP (0.1 mM)	51
−CTP, +CDP (1 mM)	∼1.5

ND, activity not detected, less than three turnovers per G• over 10 min.

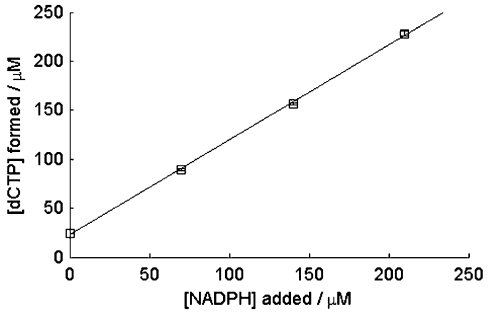

Fig. 3. Amount of 5-[^{3}H]-dCTP formed after incubation of NbNrdD with 5-[^{3}H]-CTP, dATP, TrxA, TrxB, and limiting amounts of NADPH at 30 °C for 3 h. Stoichiometry of dCTP produced per NADPH added is 0.97. The concentration of NbNrdD G• in the reaction is ~1 μM, and the ~26 turnovers per G• that occur without addition of NADPH are attributed to the reduction of TrxA by residual DTT carried over from the NbNrdD storage buffer (~27 μM).

9.3 U/mg (~2.5 min^{-1} per G•). No dCTP is detected, and the same amount of Cyt is produced in the presence or absence of the Trx system. A control with WT-NbNrdD shows no Cyt release either in the presence or absence of TrxA/TrxB/NADPH.

Crystal Structure of TmNrdD Allows Modeling of Active Site Residues in Redoxin-Dependent NrdDs. Bioinformatics analysis (described subsequently) suggested that in addition to the three cysteines in the active site, a glutamate will also be present. To determine if these residues are located in the active site of this class of redoxin-dependent NrdDs, we wanted to obtain a structure of a representative of this NrdD subtype. Selenomethionine (SeMet)-labeled NrdD from *T. maritima* (TmNrdD), which is related to NbNrdD (30% sequence identity; Fig. S1), was successfully crystallized (Table S1), and the structure was solved by single-wavelength anomalous dispersion to 1.64-Å resolution. We observe a $(\beta/\alpha)_{10}$ barrel architecture similar to the T4 bacteriophage class III RNR (29) [root mean square deviation (RMSD), 2.5 Å], including the C-terminal G• domain and Zn-binding site (Fig. S4*A*) but with four additional helices at the N terminus (Fig. 5*A* and Fig. S4*B*). The Cys loop containing essential cysteines C329 and C330 (equivalent to C300 and C301 in NbNrdD), however, is not present in its expected conformation within the barrel. In fact, residues 330–349 are not visible in the electron density map in either monomer, and SDS/PAGE analysis of the crystals indicates that protein cleavage occurs within this stretch of amino acids (Fig. S5). The molecular weights of the fragment bands (39 and 36 kDa) suggest that the missing density may be due to disorder around a single cleavage site rather than a missing stretch of residues. Regardless, cleavage within residues 330–349 has a dramatic affect; adjacent residues 320–329 and 350–365 move, and residues 350–365, which show no sequence or structural similarity to the Cys loop, now occupy the Cys loop position (Fig. 5*B*). Despite the absence of the Cys loop in our structure, the barrel architecture is intact, and the G• domain is ordered. The C terminus beyond the G• loop is also ordered but adopts two distinct conformations in the two different molecules in the asymmetric unit (Fig. 5*C*).

Using the TmNrdD structure and T4 bacteriophage NrdD structure [Protein Data Bank (PDB) ID code 1H79] (45), we constructed a hybrid structural model (Fig. 6*A*). The Cys loop was modeled from T4 NrdD (T4 residues 287–293; equivalent to TmNrdD 327–333). Because there are no structures of a nucleoside triphosphate-bound RNR, CTP was modeled in the active site based on the position of CDP in the *T. maritima* class II RNR (NrdJ) (PDB ID code 1XJN) (46). Structural superpositions based on aligning residues in the β strands surrounding the active site yield all-atom RMSD values between TmNrdD and T4 NrdD of 0.9 Å and between TmNrdD and *T. maritima* NrdJ of 2.0 Å.

In the TmNrdD model, C330 is positioned at the tip of the Cys loop to initiate catalysis (Fig. 6*A*). The modeled C329 is directly adjacent to C125 (Cβ–Cβ distance, 3.8 Å), sufficiently close to form the proposed disulfide (Fig. 1*B*), as occurs in *E. coli* class Ia (Cβ–Cβ distance, 4.1 Å) and *T. maritima* class II enzymes (Cβ–Cβ distance, 4.2 Å) (Fig. 6*B*). The precise orientation of the Cys loop and the placement of C329 in relation to the ribose of the CTP cannot be determined from this model, but the general locations of C329 and C125 are consistent with their proposed mechanistic role. In the class Ia RNR from *E. coli*, reduction of the ketyl radical intermediate (Fig. 1*A*, **3**) is proposed to occur by hydrogen atom transfer from C225 from the bottom face of the nucleotide, followed by eventual disulfide formation with C462 (Fig. 1*B*), which is deeply buried on the innermost side of the active site. TmNrdD C125 is observed in the crystal structure to be positioned equivalently to *E. coli* class Ia C225, consistent with it playing the same catalytic role. However, TmNrdD does not have a cysteine equivalent to *E. coli* class Ia C462 in the rear of the active site; S368 occupies this space in the structure. Instead, the location of C329 on the Cys loop requires formation of the disulfide at the front of the active site, in an orientation distinct from the class I/II enzymes, possibly in a position to facilitate its rereduction by redoxins (discussed below).

The reduction of the 3′-keto-deoxynucleotide (Fig. 1*B*, **4**) requires a proton in addition to the electron from the disulfide radical anion. We proposed from sequence alignments that residue E495 could function as the proton source, taking the place of E441 in the *E. coli* class Ia RNR. This glutamate is not conserved in the *E. coli*-type NrdD, but is conserved in the *T. maritima*-type NrdD (Fig. 7 and *Discussion*). Here we find that the location of E495 in the TmNrdD structure overlaps quite well with the position of E441 (Fig. 6*A*). Unfortunately, the mutant of the corresponding residue in NbNrdD, E438Q, displayed low G• content, and the enzyme was inactive in forming either dCTP or Cyt, which prevented us from carrying out experiments analogous to the *E. coli* NrdA(E441Q) mutant (28, 47).

A major puzzle with respect to this newly discovered class III RNR subtype is how the active site disulfide, which must be formed on each round of catalysis, is rereduced by a redoxin. The class I and II RNRs require five cysteine residues for catalysis: three in the active site (Fig. 1*B*) and two located in the C-terminal tail (Fig. 1*D*) that are involved in rereduction of the disulfide generated during dNDP (dNTP) formation so that multiple turnovers can occur. All class III RNRs lack a C-terminal tail containing a pair of cysteines (27) that could function in this capacity. The TmNrdD structural model shows that C329 and C125 are found at the outer edge of the active site, in contrast to the deeply buried cysteine pair found in the class I/II enzymes. Nonetheless, a large conformational

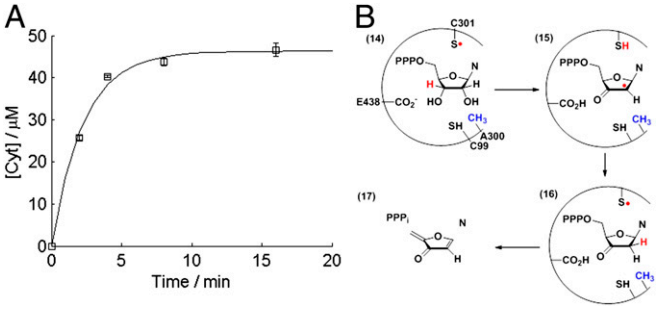

Fig. 4. (*A*) Time-dependent 5-[^{3}H]-Cyt release in the reaction of NbNrdD (C300A) with 5-[^{3}H]-CTP. The concentration of G• in the reaction is ~8 μM. (*B*) Proposed mechanism for Cyt release by NbNrdD(C300A).

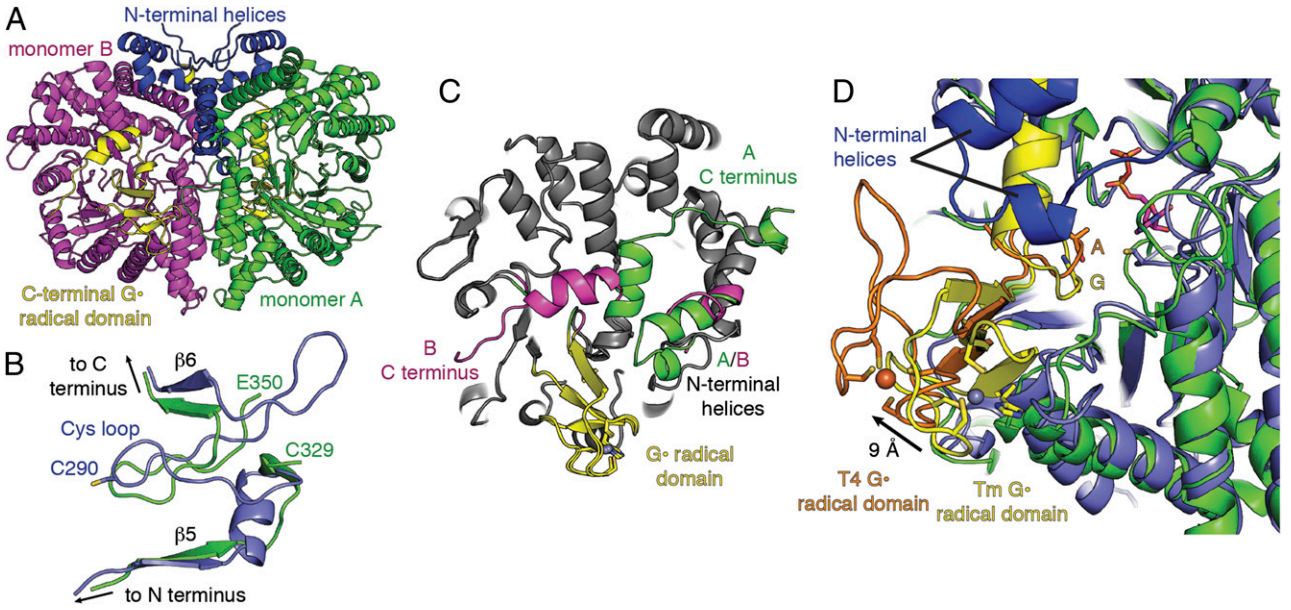

Fig. 5. Overall structure of *T. maritima* class III RNR. (*A*) The structure of the dimer is shown with monomer A (green) and monomer B (magenta) joined by an interface that contains four N-terminal helices specific to TmNrdD (blue). (*B*) Superposition of residues 265–312 of the T4 bacteriophage structure (PDB ID code 1H79) (45), which includes the Cys loop (blue), with residues 314–329 and 350–369 of the TmNrdD structure (green). Residues 350–365 of TmNrdD occupy the position left vacant by the absence of the Cys loop (residues 324–334). (*C*) Monomers of TmNrdD differ by more than 1 Å in two regions: the tip of the N-terminal helices that contact the G• domain and the C-terminal helix (green, monomer A; magenta, monomer B). The core of the protein is unchanged (gray). (*D*) G• domains of TmNrdD (yellow, Gly shown in sticks) in both chains are positioned further inside the barrel relative to that of T4 bacteriophage (orange, G580A in sticks). The C-terminal helix of TmNrdD is shown in its monomer A orientation (yellow). Zinc (TmNrdD, gray) and iron (T4 phage, orange) atoms, from Tm and T4 structures, respectively, are shown as spheres. CDP (magenta) is modeled based on the *T. maritima* class II RNR structure (PDB ID code 1XJN) (46). *C* and *D* are reproduced in Fig. S4 *C* and *D* as stereoimages.

change would seem be required to allow the direct access of TrxA to the oxidized cysteine pair. The active site in our structure is buried primarily by the presence of the G• domain and two N-terminal helices specific to the TmNrdD-type enzymes. Although the active site appears buried, the $(\beta/\alpha)_{10}$ barrel architecture conserved in all classes of RNRs and all G• enzymes is known to undergo conformational changes that can either close or expose the active site. In the class II RNR from *Lactobacillus leichmannii*, coenzyme B_{12} binding causes a shift in a small number of residues exterior to the barrel, which closes the barrel and shields the cofactor from solvent (48). In PFL, the G• domain must exit the active site to become accessible to its partner activating enzyme for radical generation, and circular dichroism spectroscopy shows that binding of PFL to its activase is accompanied by enhanced enzyme conformational flexibility (49, 50). The recent structure of the G• enzyme benzylsuccinate synthase (51) reveals a clamshell-like opening of the barrel, allowing release of the G• domain from the interior of the protein, which would again allow for G• formation. In this work, support for the proposal that the G• domain is flexible comes from the observation that the domain position in TmNrdD is shifted by 9 Å (~15° rotation) relative to that of T4 bacteriophage (Fig. 5*D*). Although the relevance, if any, of this shift is not established at this time, it illustrates the wide range of motion available to the G• domain in class III RNRs. Also notable for understanding active site access in TmNrdD is the observation that the G• domain C-terminal helix has two distinct conformations (Fig. 5*C*): in monomer A, the helix is extended and completely blocks active site access; in monomer B, the helix kinks and wraps around the protein, similar to other G• enzymes, revealing an opening to the active site. Although this active site cavity is not large enough to accommodate thioredoxin, the flexibility observed in the C- and N-terminal helices, as well as in the G• domain, indicates the likelihood that further opening of the active site that would permit rereduction by thioredoxin.

Bioinformatics Analysis Suggests Three Chemically Distinct NrdD Subtypes. Further support for the existence of distinct subtypes of NrdDs was obtained by a bioinformatics analysis. A phylogenetic tree of NrdDs (Fig. 7*B*) was constructed using 59 sequences from the RNRdb (33), chosen to include phylogenetically and metabolically diverse bacteria and archaea. Analysis of the conserved residues proposed to be important for chemistry [the three active site cysteines Cys(1–3), Met, and Glu in Fig. 7*A*] led us to propose that there are three chemically distinct NrdD subtypes that we label NrdD1, NrdD2, and NrdD3. The top face Cys(1) on the Cys loop and the bottom face Cys(2) are conserved in all NrdDs, and Cys(3), Met, and Glu are variously conserved in the different NrdD subtypes. The phylogeny of these NrdDs suggests that horizontal gene transfer plays a large role in accounting for their distribution among the diverse bacteria and archaea, as postulated for all classes of RNR (18).

NrdD1 includes the previously studied bacteriophage T4, *E. coli*, and *L. lactis* enzymes that use formate as a reductant (4). Met, thought to play a role in the reaction with formate (Fig. 1 *A* and *C*) (31), is conserved in all NrdD1s. None of the NrdD1 sequences examined have the Cys(3) and the Glu. NrdD1s are present almost exclusively in fermentative bacteria, which have a PFL, and in hydrogenotrophic methanogens, where the F420-dependent formate dehydrogenase provides a pathway for formate generation (52). In certain fermentative bacteria, like *E. coli* and *L. lactis*, PFL plays a role in energy metabolism by converting pyruvate to acetyl-CoA, which leads to ATP production via acetyl phosphate, and formate, which is a waste product (16). In some bacteria, PFL also plays a role in providing C1 intermediates for biosynthesis (53, 54).

NrdD2 includes the enzymes from *N. bacilliformis* and *T. maritima*, which are proposed to obtain reducing equivalents from a redoxin. In these proteins, three Cys(1–3) and a Glu, which enable nucleotide reduction via disulfide chemistry (Fig. 1 *A* and *B*), are conserved. In these enzymes, Met is often present but is not conserved.

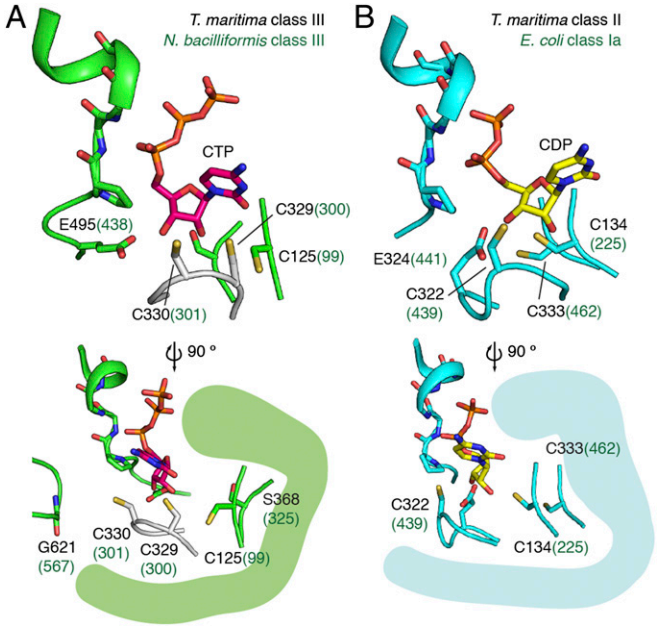

Fig. 6. Model for disulfide formation in class III RNR. (*A*) The crystal structure of TmNrdD is shown in green (the inserted loop, residues 350–365, is not shown for clarity). The Cys loop based on bacteriophage T4 NrdD (PDB ID code 1H79) (45) has been modeled in white. CTP has been modeled based on the *T maritima* class II RNR structure (magenta). The side view shows the position of the G• loop. (*B*) The structure of CDP (yellow) bound *T. maritima* class II RNR (PDB ID code 1XJN) (46).

In NrdD2s lacking Met, this position is most commonly occupied by Ser, as in NbNrdD and TmNrdD, but also Ala, Glu, or Phe in some deeply rooted bacteria and archaea. The residue corresponding to the catalytic E441 in *E. coli* NrdA (Fig. 1 *A* and *B*), which is expected to be close to the formate binding site, is replaced with either Ser or Thr in NrdD1s. However, in NrdD2s, it is replaced with Ile, Leu, or Phe, which may hinder the access of formate. In contrast to the restricted distribution of NrdD1, NrdD2 is present in nonmethanogenic archaea and in bacteria with diverse types of anaerobic metabolism. In support of the nature of the proposed reductant, several organisms have NrdD2s with associated redoxins, including *Acetobacterium woodii* (55), in the form of a C-terminal fusion to NrdD2, and *Desulfarculus baarsii* (56) and *Methanomassiliicoccus luminyensis* (57), which have a thioredoxin-like protein in the operon.

NrdD3, present only in certain methanogens and the closely related *Archaeoglobi* (58), shows important differences with respect to NrdD1 and NrdD2. Although they share up to 50% pairwise sequence identity with NrdD1s from other methanogens, they lack Met. Also, although they contain all three Cys (1–3) like the NrdD2s, they lack Glu. Additional observations support the designation of a third NrdD subtype and that these proteins will possess RNR activity. NrdD3s all contain the G• consensus sequence, and some of them (e.g., *Archaeoglobus veneficus*) contain an N-terminal ATP cone domain. In some sequenced organisms, NrdD3 is the only annotated RNR (e.g., *Archaeoglobus profundus, Methanospirillum hungatei*), although other organisms also contain a NrdJ. Interestingly, some NrdD3s (*Archaeloglobus veneficus, Methanoscarcina barkerii*) are found in the same operon as a thioredoxin-like protein.

The designation of the three NrdD subtypes largely correspond to the phylogeny of the protein (Fig. 7*B*), with the exception of a deeply rooted branch containing *M. luminyensis*, *Aminomonas paucivorans*, and *Kuenenia stuttgartiensis* NrdD2. An additional observation suggesting the existence of NrdDs with distinct types of chemistry is that, although it is uncommon for a single organism to contain two copies of the same NrdD subtype, there are many organisms that contain both NrdD1 and NrdD2 (e.g., *Shewanella sediminis, Bacteroides ovatus*, and *Elusimicrobium minitum*). We hypothesize that these class III RNR variants are used under different anaerobic growth conditions, similar to the case of the class Ia and Ib RNRs in *E. coli*.

Discussion

Because of their essential role in the de novo production of deoxynucleotides, RNRs are ubiquitous enzymes in nearly all cellular organisms and many viruses (18, 33, 59). The complex chemistry involved in nucleotide reduction requires initial generation of a transient thiyl radical. The class of RNR used by an organism reflects the mechanism of this radical formation and a combination of factors including the presence or absence of oxygen (60) and availability of metals (61). Here we report the discovery of a subtype of class III RNR in *N. bacilliformis* where, like the class I and II RNRs, nucleotide reduction is facilitated by a redoxin, which is a ubiquitous protein found in all organisms. This proposed reliance on a redoxin is unlike the class III RNRs studied to date that couple nucleotide reduction to the oxidation of formate, a metabolite produced by some but not all organisms as part of their primary metabolism.

Biochemistry, Structure, and Bioinformatics Support the Existence of a Second NrdD Subtype. The cloning of *N. bacilliformis* class III RNR was motivated by a bioinformatics analysis, which led to the identification of a potential second NrdD subtype containing three cysteines necessary to carry out nucleotide reduction via a mechanism analogous to that of the class I and II RNRs (Fig. 1 *A* and *B*). Our biochemical investigations showed that NbNrdD catalyzes the reduction of NTPs, which are also the substrates of formate-dependent class III RNRs. DeoxyNTP formation required the presence of the TrxA/TrxB/NADPH system but not formate, and the 1:1 stoichiometry of NADPH consumption and dCTP production demonstrates that the reducing equivalents for dCTP generation are provided by the Trx system.

As predicted, the NbNrdD(C301A) mutant is inactive because no initiating thiyl radical can be produced. In support of the active site disulfide between C99 and C300 (Fig. 1*B*), our structural modeling using the related TmNrdD enzyme as the molecular scaffold is consistent with these cysteines being close enough to form a disulfide bond. Furthermore, the NbNrdD (C300A) mutant behaves like the *E. coli* class Ia RNR C462A mutant in that reaction with substrate (CTP in the case of NbNrdD) results in the formation of Cyt (Fig. 4*B*), showing that the mutant is competent for formation of a 3′-keto-dCTP intermediate but unable to carry out nucleotide reduction. Thus, our assays establish the presence of a second NrdD subtype that is distinct from *E. coli* NrdD in being able to use thioredoxin rather than formate as a reductant for nucleotide reduction.

Distribution of NrdD Subtypes Correlates with Metabolism. Our bioinformatics study revealed that there are in fact three NrdD subtypes (NrdD1, NrdD2, and NrdD3), the distribution of which shows a striking correlation with the organism's anaerobic metabolism. Among bacteria, NrdD1 is localized almost exclusively in fermentative bacteria that use PFL. An interesting exception is the deep branching *Elusimicrobium minitum* (termite group 1; Fig. 7*B*) (62), which has two NrdD subtypes (NrdD1 and NrdD2) but no PFL: its NrdD1 operon contains a ^{10}*N*-formyl-tetrahydrofolate synthetase as a possible source of formate. In contrast, NrdD2 is present in bacteria carrying out a diverse range of anaerobic metabolism.

Although it is tempting to explain the distribution of NrdD subtypes by the availability of intracellular formate, a counterexample is provided by acetogens: although formate is an

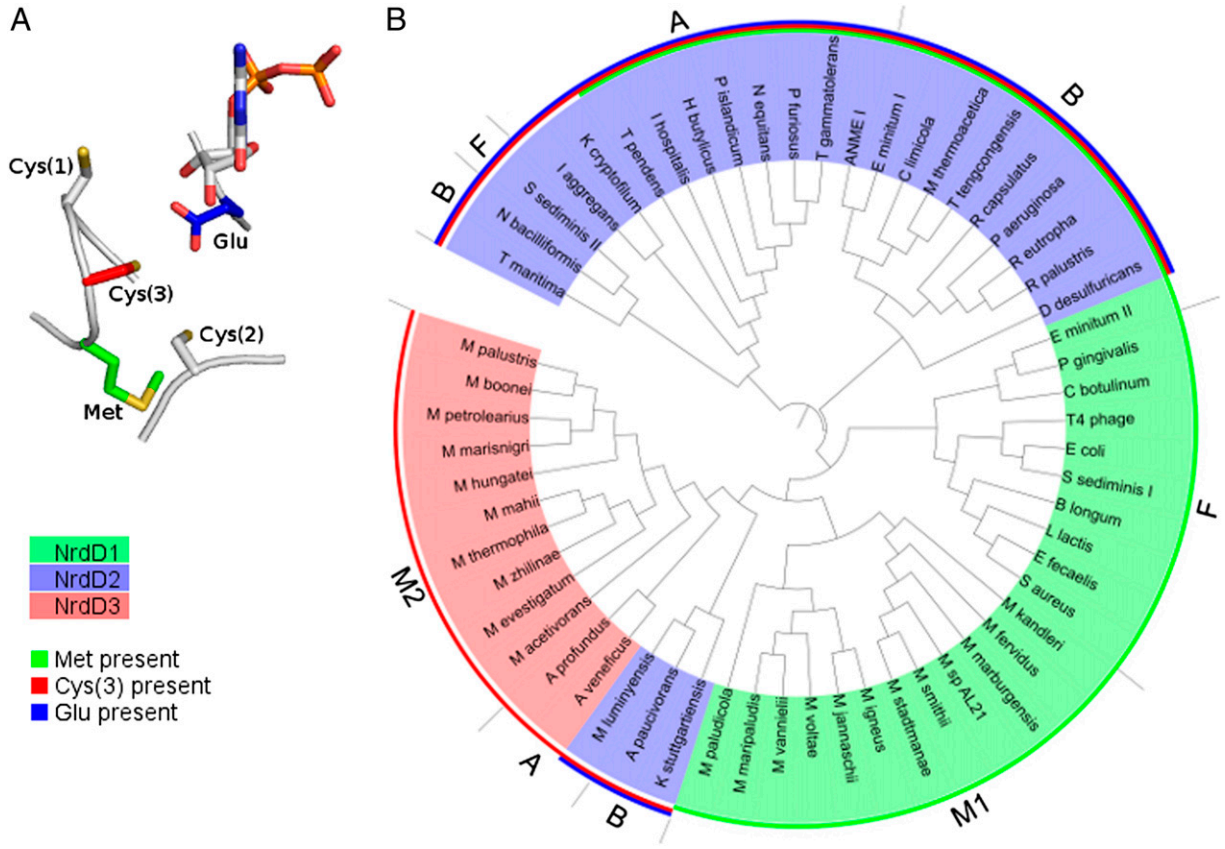

Fig. 7. (*A*) Model of a generic NrdD active site showing residues proposed to be important for chemistry. Cys(1) and Cys(2) are conserved in all NrdDs, and Met, Cys(3), and Glu are variously conserved in the different NrdD subtypes. (*B*) Phylogenetic tree of NrdDs. NrdD subtypes are indicated by highlighting (green = NrdD1, blue = NrdD2, red = NrdD3). Presence of Met, Cys(3), and Glu are indicated by colored bars (green, red, and blue, respectively) along the circumference of the plot. F, bacteria with PFL; B, other bacteria; M1, type I methanogens that use the cytosolic electron-bifurcating heterodisulfide reductase; M2, other methanogens; A, other archaea.

intermediate of acetogenesis (63), acetogens invariably contain NrdD2. Instead we hypothesize that the energy metabolism of the organism and the redox window that it inhabits determines whether it is more thermodynamically efficient to use formate or other reductants for nucleotide reduction. In fermentative bacteria, formate is produced by PFL as a waste product; thus, NrdD1 may be preferred. In contrast, in bacteria that carry out anaerobic respiration, formate is not known to be produced as part of their energy metabolism, and oxidation of any available formate from the environment can be coupled to the generation of ATP, which rationalizes why NrdD2 may be preferred. In acetogens, coupling of ribonucleotide reduction by NrdD2 to the TrxA/TrxB system could provide oxidized pyridine nucleotides that are substrates for energy conservation (55).

All archaea examined contain exclusively NrdD2, except for methanogens and their relatives, which contain either NrdD1 or NrdD3. In the case of the methanogens, the NrdD subtype used correlates with its mechanism for energy conservation (64), which is in turn related to its formate metabolism. NrdD1 is present only in type I hydrogenotrophic methanogens that carry out energy conservation by means of the cytosolic electron-bifurcating heterodisulfide reductase (64). The type I methanogens examined contain the F420-dependent formate dehydrogenase (52) as a possible means of synthesizing formate, and many can carry out methanogenesis with formate as a substrate. Apart from ribonucleotide reduction, the other known role of formate in the primary metabolism of type I methanogens is in purine biosynthesis, in an ATP-dependent reaction with formate to form formylphosphate catalyzed by PurT (glycineamide ribonucleotide synthetase) (65, 66), suggesting the presence of intracellular formate. A case in point is *Methanocella paludicola* (rice cluster I) (67), a methanogen with cytochromes that nevertheless uses the type I pathway for methanogenesis (64), and contains NrdD1.

Other methanogens, including methylotrophic and acetoclastic methanogens that carry out energy conservation by other means, and their relatives, the sulfate-reducing *Archaeoglobi*, use NrdD3 instead. Unlike type I methanogens, these organisms are unable to use formate as a substrate for methanogenesis, and several sequenced members (e.g., *Methanosarcina acetivorans* and *Methanosarcina mazei*) do not contain formate dehydrogenase (68). They carry out purine biosynthesis in a manner dependent not on formate, but on ^{10}N-formyl-tetrahydrofolate, catalyzed by PurN (glycineamide ribonucleotide synthase) (65), suggesting that formate may not be present in the cell. Although many NrdD3 operons contain a redoxin, methanogens lack a conserved thioredoxin reductase, and the origin of the reducing equivalents for NrdD3 is unclear, but could be linked to the heterodisulfide reductase system common to these organisms.

Several interesting methanogens and relatives also possess NrdD2. The obligate methylotroph *Methanococcoides burtonii* (69) has both NrdD2 and NrdD3, suggesting that the source of reducing equivalents for these two RNRs may be different. The methanogen relative ANME-1 (70, 71), which carries out anaerobic methane oxidation, has NrdD2 but no NrdD3, in conjunction with its unique metabolism. *Methanomassiliicoccus luminyensis* (57), which carries out methanogenesis from methanol but is a relative of the nonmethanogenic *Thermoplasmatales*,

contains a deeply rooted NrdD2 with an associated redoxin in the operon. Because of the central role of formate and thiols in many anaerobic processes, the distribution of class III RNRs among different organisms may shed light on aspects of anaerobic biochemistry, particularly in organisms that are unculturable.

A Clue Regarding the Ancestral NrdD. RNR has been proposed to provide the link between the RNA and DNA worlds (72, 73), with the class III RNR proposed to precede the class I and II enzymes. Given the central role of formate and thiols in many anaerobic processes, the identity of the original NrdD has implications regarding the metabolism of the first organism with a DNA genome. Unfortunately, the NrdD1 and NrdD2 sequences are too divergent to allow us to convincingly root the NrdD phylogenetic tree. However, we note that the residue Met (Fig. 7*A*) proposed to be involved in formate chemistry in NrdD1 (31) is also present in many but not all NrdD2s, possibly as an evolutionary relic, suggesting that NrdD1 may precede NrdD2. If true, this suggests that formate is present in the ancestral organism, possibly as an intermediate in an ancient Wood–Ljungdahl pathway (55).

Materials and Methods

For additional details, see *SI Text*.

Cloning, Expression, and Purification of NbNrdD, NbNrdG, and TmNrdD. Details are provided in *SI Text*. *N. bacilliformis nrdD* and *nrdG* were obtained by PCR from genomic DNA (gift from Xiang-Yang Han, University of Texas M. D. Anderson Cancer Center, Houston), and *T. maritima nrdD* was obtained by PCR from genomic DNA (gift from Kenneth Noll, University of Connecticut, Storrs, CT). The genes were cloned into pET28a-NbNrdD, pET28a-NbNrdG, and pET28a-TmNrdD vectors (Novagen) with primers described in Table S2. To increase soluble expression, *N. bacilliformis nrdG* was later cloned into pSV272 to give pMBP-NbNrdG, which contains an N-terminal maltose-binding protein (MBP) fusion with an N-terminal His_6-tag. The procedure for expression of [SeMet]-labeled TmNrdD for crystallography was adapted from existing protocols (74). All proteins were purified by TALON (Clontech) chromatography (Fig. S6). The final yield was ∼10 mg/g cells for NbNrdD ($\varepsilon_{280} = 73{,}410\ M^{-1}\cdot cm^{-1}$), ∼1 mg/g cells for MBP-NbNrdG ($\varepsilon_{280} = 95{,}760\ M^{-1}\cdot cm^{-1}$), and ∼2 mg/g cells for [SeMet]-TmNrdD ($\varepsilon_{280} = 106{,}830\ M^{-1}\cdot cm^{-1}$).

Reconstitution of the NbNrdG [4Fe4S] Cluster. The procedure was carried out in a MBraun anaerobic chamber. Solutions of Na_2S and of $Fe(NH_4)_2(SO_4)_2$ in water (100 mM) were freshly prepared in the anaerobic chamber. A solution of MBP-NbNrdG (200 μM, 0.3 mL) was made anaerobic on a Schlenk line and brought into the glovebox. A solution of DTT (1 M) was added to 10 mM, followed by ordered addition of the solution of Na_2S (5 equivalents) and $Fe(NH_4)_2(SO_4)_2$ (5 equivalents). The mixture was incubated for 12 h at 4 °C. EDTA (5 eq.) was then added, and the solution was desalted using a Sephadex G-25 column (1 × 9 cm, 7 mL) equilibrated with Tris buffer (20 mM, pH 7.5). The final material typically contained ∼2.5 atoms of Fe per peptide determined by the ferrozine assay (75).

Generation of the NbNrdD G•. In a 1.5-mL polypropylene Eppendorf tube, a 50-μL mixture of NbNrdD (40 μM), NbNrdG (20 μM), SAM (0.5 mM), Bicine potassium salt, pH 7.5 (30 mM), and acriflavin (10 μM) was placed 1 m away from a fluorescent lamp in the glovebox at 15 °C for 3 h. For inspection by X-band EPR spectroscopy, the solution was diluted to 200 μL with Tris buffer (20 mM, pH 7.5) and 5% (vol/vol) glycerol to give a final concentration of 10 μM NbNrdD and sealed in an EPR tube with a rubber stopper. The solution was quenched in liquid N_2 immediately after removal from the glovebox. The amount of G• in the solution was determined by comparing the EPR signal intensity to that of a $CuSO_4$ standard (76). A typical yield of 0.25–0.30 radicals per NbNrdD polypeptide was reproducibly obtained.

X-Band EPR Spectroscopy. Continuous wave X-band EPR spectra were recorded at 77 K in the Massachusetts Institute of Technology Department of Chemistry Instrumentation Facility on a Bruker ESP-300 X-band spectrometer equipped with a quartz finger Dewar filled with liquid N_2. Experimental conditions were as follows: microwave frequency, 9.45 GHz; modulation amplitude, 0.15 mT; modulation frequency, 100 kHz; time constant, 5.12 ms; scan time, 41.9 s; microwave power, 20 μW.

Preparation of [^{2}H]-Gly–Labeled NbNrdD to Establish the Location of the Radical on Glycine. The procedure was identical to the preparation of [SeMet]-TmNrdD, except that instead of SeMet, the culture contained L-methionine (50 mg/L) and [^{2}H]-glycine (6 mM, 98% isotopic enrichment; Cambridge Isotope Labratories). The yield was ∼1 g of cell paste, and purification was carried out according to the procedure described for the unlabeled protein. The EPR sample was then prepared as described above.

Assay for Solvent-Exchangeable Glycine H_α Protons. Tris buffer (20 mM, pH 7.5) was prepared in D_2O (99.9%; Cambridge Isotope Laboratories) in the glovebox. NbNrdD and NbNrdG were exchanged into this buffer by repeated dilution and concentration by ultrafiltration (Amicon YM-30), such that <1% H_2O remained, and were incubated for 12 h at 4 °C to allow for proton exchange. The activation reaction was carried out as described above, but with all components made up in D_2O in the glovebox, followed by preparation of the EPR sample as described above.

Activity Assay for dCTP Formation by NbNrdD. The assay mixture contained (in 100 μL) NbNrdD (4 μM, ∼1 μM G•), ATP (1 mM), 5-[^{3}H]-CTP (1 mM, 4,170 cpm/nmol), *E. coli* TrxA (30 μM), *E. coli* TrxB (1 μM), and NADPH (1 mM) in assay buffer (30 mM Tris, pH 7.5, 30 mM KCl, and 10 mM $MgSO_4$) and was incubated at 30 °C. Aliquots (20 μL) were removed at 2-min intervals and quenched with 2% (vol/vol) perchloric acid (20 μL). Subsequent to removal of the phosphates using calf intestine alkaline phosphatase (Roche), dCTP formation was analyzed by the method of Steeper and Steuart (77). One unit of activity is equivalent to 1 nmol of dCTP per minute. The specific activity of NbNrdD is 49 U/mg NrdD protein (∼0.24 s^{-1} per G•).

Stoichiometry of NADPH Consumption and dCTP Production. The assay mixture was divided into 20-μL aliquots containing NbNrdD (4 μM, ∼1 μM G•), dATP (0.1 mM), 5-[^{3}H]-CTP (1 mM, 4170 cpm/nmol), *E. coli* TrxA (5 μM), *E. coli* TrxB (1 μM), and NADPH (0, 70, 140, or 210 μM) in assay buffer and was incubated at 30 °C for 3 h to allow for complete consumption of NADPH. Workup of the samples was carried out as described above to quantify the dCTP formed.

Activity Assay for Cytosine Release by NbNrdD(C300A). The assay mixture contained (in 100 μL) NbNrdD(C300A) (33 μM, ∼8 μM G•) and 5-[^{3}H]-CTP in assay buffer and was incubated at 30 °C. Aliquots (20 μL) were removed at 2, 4, 8, and 16 min and quenched with 2% (vol/vol) perchloric acid (20 μL). dCTP formation was analyzed by the method of Steeper and Steuart (77). Formation of Cyt was analyzed by passing the mixture through an anion exchange column to remove the nucleoside triphosphates as previously described (31).

To a 7-mL portion of the eluate of the Dowex-1-borate column was added carrier Cyt and dC (10 nmol each). The mixture was concentrated by lyophilization, redissolved in water, and cooled on ice, and the precipitated borate salts were removed by centrifugation. The supernatant was analyzed by HPLC using an Alltech Econosil column (C18, 10 μm, 250 × 4.6 mm) on a Waters 515 HPLC system equipped with a 2,996 photodiode array detector. The compounds were eluted with KPi (20 mM, pH 6.8) at a flow rate of 1.0 mL/min. Fractions were collected (0.5 mL) and analyzed by scintillation counting. Cyt was identified by coelution with a standard at 5 min (Fig. S3).

Crystallization and Crystal Structure of TmNrdD. Crystals of SeMet-TmNrdD were grown aerobically by sitting drop vapor diffusion at 21 °C. Protein, with the His-tag intact, at 13 mg/mL in a buffer containing 25 mM Hepes, pH 7.6, 15 mM $MgCl_2$, 20 mM KCl, 0.5 mM Tris(2-carboxyethyl)phosphine (TCEP), 1 mM dGTP, and 5 mM ATP, was screened against commercial screens (Hampton Research, Microlytic, and Qiagen) at a 1:1 ratio of protein to precipitant. A Phoenix pipetting robot (Art Robbins Instruments) was used for dispensing 150-nL drops in screening trays. Diffraction quality crystals grew over several weeks in wells containing 0.085 M trisodium citrate, pH 5.6, 0.17 M ammonium acetate, 25.5% (wt/vol) PEG 4000, and 15% (vol/vol) glycerol. Crystals were flash frozen in liquid nitrogen without additional cryoprotection.

The structure of TmNrdD was solved by single-wavelength anomalous dispersion. A 1.64-Å resolution Se peak anomalous dataset (12664.1 eV) was collected at the Advanced Photon Source using a minikappa goniometer to collect Friedel pairs on a single image. Data were collected on a Pilatus 6M detector (Dectris). The data were indexed and scaled with HKL2000 (78) in space group $P2_1$ with unit cell constants a = 78.3, b = 98.8, c = 86.6, and β = 111.7. The resulting unit cell volume of 622,000 $Å^3$ is consistent with two molecules per asymmetric unit with a solvent content of ∼40% (statistics found in Table S1). Forty-five initial Se sites were found with SHELXD in the package HKL2MAP (79) with a resolution cutoff of 2.1 Å ($d''/sig = 0.8$). The

resulting sites were refined using data to 1.8-Å resolution, and density modification was performed in Phenix AutoSol (80), yielding the phasing statistics shown in Table S1. The resulting maps at 1.8-Å resolution were adequate for chain tracing and manual building of the entire protein model and surrounding water molecules in Coot (81). The resolution was increased to 1.64 Å, and iterative refinement of the model was performed with phenix.refine. Composite omit maps were used to verify residue and ligand placement. All native residues are present at the N and C termini of chain A; chain B is missing three C-terminal residues. Both chains have additional density at the N terminus corresponding to eight residues of the thrombin cleavage site and linker; no residues of the His-tag are observed, although the His-tag was not cleaved before crystallization. Residues 54–62 of chain A are unstructured. Residues 330–349 of chain A and 328–350 of chain B are not observed in the density at all as a consequence of peptide bond cleavage near residue 330 (Fig. S5). The final model contained 98.3% of residues in the favored region of the Ramachandran plot, with 1.6% in additionally allowed regions and 0.08% (1 residue, G621) disallowed. G621 is converted in to the G• and thus is expected to adopt a slightly strained conformation in the unactivated protein. Figures were created in PyMOL Version 1.4.1 (Schrödinger, LLC). A structural model for TmNrdD Cys loop was constructed by superimposing the structures of T4 bacteriophage (1H79) (45) and *T. maritima* class III RNR using residues in the β-barrel surrounding the active site loops. Because there are no structures of a nucleoside triphosphate-bound RNR, CTP was modeled in the active site based on the position of CDP in the class II *T. maritima* NrdJ (1XNJ) (46). The resulting hybrid model should be considered purely as a tool for guiding discussions of the possible chemistry occurring in TmNrdD and was not subjected to energy minimizations or dynamics.

Phylogenetic Analysis of NrdDs. To determine the existence of different NrdD subtypes, 59 amino acid sequences were chosen to include phylogenetically and metabolically diverse bacteria and archaea and aligned with Muscle (MEGA5 software) (82). Subsequently, a neighbor-joining phylogenetic tree (83) was generated, and the Jones-Taylor-Thornton matrix method (84) was used to determine the evolutionary distances. The unequal rate of variation among amino acid sites was modeled with a γ distribution with shape parameter of 4 (85). Additionally, a complete deletion of the sites containing gaps was used to palliate the length and divergence variation, focusing on more conserved amino acid clusters. The level of confidence for the branches was determined based on 2,000 bootstrap replicates (86). The resulting consensus tree was rendered using the web-based program iTOL (87) (Fig. 7*B*, bootstrap values presented in Fig. S7).

ACKNOWLEDGMENTS. We thank Dr. Xiang-Yang Han for the gift of *N. bacilliformis* genomic DNA, Prof. Kenneth Noll for the gift of *T. maritima* genomic DNA, and Dr. Greg Fournier, Dr. Silvan Scheller, and Prof. Rudolf K. Thauer for helpful discussions. This work was supported in part by ASTAR Singapore (Y.W.) and the National Science Foundation Graduate Research Fellowship under Grant 0645960 (to M.A.F.). C.L.D. is a Howard Hughes Medical Institute Investigator. This work is based on research conducted at the Advanced Photon Source on the Northeastern Collaborative Access Team beamlines, which are supported by National Institutes of Health (NIH) Award GM103403 from the National Center for Research Resources. Use of the Advanced Photon Source is supported by the US Department of Energy, Office of Basic Energy Sciences, under Contract DE-AC02-06CH11357. This work was supported by NIH Grant GM29595 (to J.S.).

1. Fontecave M, Eliasson R, Reichard P (1989) Oxygen-sensitive ribonucleoside triphosphate reductase is present in anaerobic *Escherichia coli*. *Proc Natl Acad Sci USA* 86(7):2147–2151.
2. Sun X, et al. (1996) The free radical of the anaerobic ribonucleotide reductase from *Escherichia coli* is at glycine 681. *J Biol Chem* 271(12):6827–6831.
3. Nordlund P, Reichard P (2006) Ribonucleotide reductases. *Annu Rev Biochem* 75: 681–706.
4. Mulliez E, Ollagnier S, Fontecave M, Eliasson R, Reichard P (1995) Formate is the hydrogen donor for the anaerobic ribonucleotide reductase from *Escherichia coli*. *Proc Natl Acad Sci USA* 92(19):8759–8762.
5. Hofer A, Crona M, Logan DT, Sjöberg B-M (2012) DNA building blocks: Keeping control of manufacture. *Crit Rev Biochem Mol Biol* 47(1):50–63.
6. Stubbe J (1998) Ribonucleotide reductases in the twenty-first century. *Proc Natl Acad Sci USA* 95(6):2723–2724.
7. Sofia HJ, Chen G, Hetzler BG, Reyes-Spindola JF, Miller NE (2001) Radical SAM, a novel protein superfamily linking unresolved steps in familiar biosynthetic pathways with radical mechanisms: Functional characterization using new analysis and information visualization methods. *Nucleic Acids Res* 29(5):1097–1106.
8. Gambarelli S, Luttringer F, Padovani D, Mulliez E, Fontecave M (2005) Activation of the anaerobic ribonucleotide reductase by S-adenosylmethionine. *ChemBioChem* 6(11):1960–1962.
9. Holmgren A (1979) Glutathione-dependent synthesis of deoxyribonucleotides. Characterization of the enzymatic mechanism of *Escherichia coli* glutaredoxin. *J Biol Chem* 254(9):3672–3678.
10. Jordan A, Åslund F, Pontis E, Reichard P, Holmgren A (1997) Characterization of *Escherichia coli* NrdH: A glutaredoxin-like protein with a thioredoxin-like activity profile. *J Biol Chem* 272(29):18044–18050.
11. Avval FZ, Holmgren A (2009) Molecular mechanisms of thioredoxin and glutaredoxin as hydrogen donors for mammalian S phase ribonucleotide reductase. *J Biol Chem* 284(13):8233–8240.
12. Young P, Ohman M, Xu MQ, Shub DA, Sjöberg BM (1994) Intron-containing T4 bacteriophage gene sunY encodes an anaerobic ribonucleotide reductase. *J Biol Chem* 269(32):20229–20232.
13. Torrents E, et al. (2000) The anaerobic (class III) ribonucleotide reductase from *Lactococcus lactis*: Catalytic properties and allosteric regulation of the pure enzyme system. *J Biol Chem* 275(4):2463–2471.
14. Sawers G, Böck A (1988) Anaerobic regulation of pyruvate formate-lyase from *Escherichia coli* K-12. *J Bacteriol* 170(11):5330–5336.
15. Knappe J, Sawers G (1990) A radical-chemical route to acetyl-CoA: The anaerobically induced pyruvate formate-lyase system of *Escherichia coli*. *FEMS Microbiol Lett* 75(4): 383–398.
16. Axley MJ, Grahame DA (1991) Kinetics for formate dehydrogenase of *Escherichia coli* formate-hydrogenlyase. *J Biol Chem* 266(21):13731–13736.
17. Torrents E, Aloy P, Gibert I, Rodríguez-Trelles F (2002) Ribonucleotide reductases: Divergent evolution of an ancient enzyme. *J Mol Evol* 55(2):138–152.
18. Lundin D, Gribaldo S, Torrents E, Sjöberg B-M, Poole AM (2010) Ribonucleotide reduction-horizontal transfer of a required function spans all three domains. *BMC Evol Biol* 10(1):383.
19. Kim BH, Gadd GM (2008) *Bacterial Physiology and Metabolism* (Cambridge Univ Press, Cambridge, UK).
20. Licht S, Stubbe J (1999) *Comprehensive Natural Products Chemistry*, eds Barton S, Nakanishi K, Meth-Cohn O, Poulter C (Elsevier Science, New York), Vol 5, pp 163.
21. Eklund H, Fontecave M (1999) Glycyl radical enzymes: A conservative structural basis for radicals. *Structure* 7(11):R257–R262.
22. Stubbe J, Ackles D (1980) On the mechanism of ribonucleoside diphosphate reductase from *Escherichia coli*. Evidence for 3′-C–H bond cleavage. *J Biol Chem* 255(17): 8027–8030.
23. Stubbe J, Ackles D, Segal R, Blakley RL (1981) On the mechanism of ribonucleoside triphosphate reductase from *Lactobacillus leichmannii*. Evidence for 3′ C–H bond cleavage. *J Biol Chem* 256(10):4843–4846.
24. Stubbe J, Ator M, Krenitsky T (1983) Mechanism of ribonucleoside diphosphate reductase from *Escherichia coli*. Evidence for 3′-C–H bond cleavage. *J Biol Chem* 258(3): 1625–1631.
25. Licht S, Gerfen GJ, Stubbe J (1996) Thiyl radicals in ribonucleotide reductases. *Science* 271(5248):477–481.
26. Andersson J, Bodevin S, Westman M, Sahlin M, Sjöberg B-M (2001) Two active site asparagines are essential for the reaction mechanism of the class III anaerobic ribonucleotide reductase from bacteriophage T4. *J Biol Chem* 276(44):40457–40463.
27. Mao SS, et al. (1992) A model for the role of multiple cysteine residues involved in ribonucleotide reduction: Amazing and still confusing. *Biochemistry* 31(40):9733–9743.
28. Lawrence CC, et al. (1999) High-field EPR detection of a disulfide radical anion in the reduction of cytidine 5′-diphosphate by the E441Q R1 mutant of *Escherichia coli* ribonucleotide reductase. *Proc Natl Acad Sci USA* 96(16):8979–8984.
29. Logan DT, Andersson J, Sjöberg B-M, Nordlund P (1999) A glycyl radical site in the crystal structure of a class III ribonucleotide reductase. *Science* 283(5407):1499–1504.
30. Andersson J, Westman M, Sahlin M, Sjöberg B-M (2000) Cysteines involved in radical generation and catalysis of class III anaerobic ribonucleotide reductase: A protein engineering study of bacteriophage T4 NrdD. *J Biol Chem* 275(26):19449–19455.
31. Wei Y, et al. (2014) A chemically competent thiosulfuranyl radical on the *Escherichia coli* class III ribonucleotide reductase. *J Am Chem Soc* 136(25):9001–9013.
32. Lenz R, Giese B (1997) Studies on the mechanism of ribonucleotide reductases. *J Am Chem Soc* 119(12):2784–2794.
33. Lundin D, Torrents E, Poole A, Sjöberg B-M (2009) RNRdb, a curated database of the universal enzyme family ribonucleotide reductase, reveals a high level of misannotation in sequences deposited to Genbank. *BMC Genomics* 10(1):589.
34. Han XY, Hong T, Falsen E (2006) *Neisseria bacilliformis* sp. nov. isolated from human infections. *J Clin Microbiol* 44(2):474–479.
35. Masliah-Planchon J, et al. (2009) Endocarditis due to *Neisseria bacilliformis* in a patient with a bicuspid aortic valve. *J Clin Microbiol* 47(6):1973–1975.
36. Wagner AF, Frey M, Neugebauer FA, Schäfer W, Knappe J (1992) The free radical in pyruvate formate-lyase is located on glycine-734. *Proc Natl Acad Sci USA* 89(3):996–1000.
37. Parast CV, et al. (1995) Hydrogen exchange of the glycyl radical of pyruvate formate-lyase is catalyzed by cysteine 419. *Biochemistry* 34(8):2393–2399.
38. Mulliez E, Fontecave M, Gaillard J, Reichard P (1993) An iron-sulfur center and a free radical in the active anaerobic ribonucleotide reductase of *Escherichia coli*. *J Biol Chem* 268(4):2296–2299.
39. Laurent TC, Moore EC, Reichard P (1964) Enzymatic synthesis of deoxyribonucleotides IV. Isolation and characterization of thioredoxin, the hydrogen donor from *Escherichia coli* B. *J Biol Chem* 239(10):3436–3444.
40. Moore EC, Reichard P, Thelander L (1964) Enzymatic synthesis of deoxyribonucleotides V. Purification and properties of thioredoxin reductase from *Escherichia coli* B. *J Biol Chem* 239(10):3445–3452.
41. Goulian M, Beck WS (1966) Purification and properties of cobamide-dependent ribonucleotide reductase from *Lactobacillus leichmannii*. *J Biol Chem* 241(18):4233–4242.

42. Reichard P (2002) Ribonucleotide reductases: The evolution of allosteric regulation. *Arch Biochem Biophys* 397(2):149–155.
43. Luttringer F, Mulliez E, Dublet B, Lemaire D, Fontecave M (2009) The Zn center of the anaerobic ribonucleotide reductase from *E. coli*. *J Biol Inorg Chem* 14(6):923–933.
44. Ge J, Yu G, Ator MA, Stubbe J (2003) Pre-steady-state and steady-state kinetic analysis of *E. coli* class I ribonucleotide reductase. *Biochemistry* 42(34):10071–10083.
45. Larsson K-M, Andersson J, Sjöberg B-M, Nordlund P, Logan DT (2001) Structural basis for allosteric substrate specificity regulation in anaerobic ribonucleotide reductases. *Structure* 9(8):739–750.
46. Larsson K-M, et al. (2004) Structural mechanism of allosteric substrate specificity regulation in a ribonucleotide reductase. *Nat Struct Mol Biol* 11(11):1142–1149.
47. Persson AL, Sahlin M, Sjöberg B-M (1998) Cysteinyl and substrate radical formation in active site mutant E441Q of *Escherichia coli* class I ribonucleotide reductase. *J Biol Chem* 273(47):31016–31020.
48. Sintchak MD, Arjara G, Kellogg BA, Stubbe J, Drennan CL (2002) The crystal structure of class II ribonucleotide reductase reveals how an allosterically regulated monomer mimics a dimer. *Nat Struct Biol* 9(4):293–300.
49. Vey JL, et al. (2008) Structural basis for glycyl radical formation by pyruvate formate-lyase activating enzyme. *Proc Natl Acad Sci USA* 105(42):16137–16141.
50. Peng Y, Veneziano SE, Gillispie GD, Broderick JB (2010) Pyruvate formate-lyase, evidence for an open conformation favored in the presence of its activating enzyme. *J Biol Chem* 285(35):27224–27231.
51. Funk MA, Judd ET, Marsh ENG, Elliott SJ, Drennan CL (2014) Structures of benzylsuccinate synthase elucidate roles of accessory subunits in glycyl radical enzyme activation and activity. *Proc Natl Acad Sci USA* 111(28):10161–10166.
52. Wood GE, Haydock AK, Leigh JA (2003) Function and regulation of the formate dehydrogenase genes of the methanogenic archaeon *Methanococcus maripaludis*. *J Bacteriol* 185(8):2548–2554.
53. Thauer R, Rupprecht E, Jungermann K (1970) The synthesis of one-carbon units from CO_2 *via* a new ferredoxin dependent monocarboxylic acid cycle. *FEBS Lett* 8(5):304–307.
54. Thauer RK, Kirchniawy FH, Jungermann KA (1972) Properties and function of the pyruvate-formate-lyase reaction in Clostridiae. *Eur J Biochem* 27(2):282–290.
55. Poehlein A, et al. (2012) An ancient pathway combining carbon dioxide fixation with the generation and utilization of a sodium ion gradient for ATP synthesis. *PLoS ONE* 7(3):e33439.
56. Sun H, et al. (2010) Complete genome sequence of *Desulfarculus baarsii* type strain (2st14). *Stand Genomic Sci* 3(3):276–284.
57. Gorlas A, Robert C, Gimenez G, Drancourt M, Raoult D (2012) Complete genome sequence of *Methanomassiliicoccus luminyensis*, the largest genome of a human-associated Archaea species. *J Bacteriol* 194(17):4745.
58. Klenk H-P, et al. (1997) The complete genome sequence of the hyperthermophilic, sulphate-reducing archaeon *Archaeoglobus fulgidus*. *Nature* 390(6658):364–370.
59. Dwivedi B, Xue B, Lundin D, Edwards RA, Breitbart M (2013) A bioinformatic analysis of ribonucleotide reductase genes in phage genomes and metagenomes. *BMC Evol Biol* 13(1):33.
60. Poole AM, Logan DT, Sjöberg B-M (2002) The evolution of the ribonucleotide reductases: Much ado about oxygen. *J Mol Evol* 55(2):180–196.
61. Cotruvo JA, Jr, Stubbe J (2012) Metallation and mismetallation of iron and manganese proteins in vitro and in vivo: The class I ribonucleotide reductases as a case study. *Metallomics* 4(10):1020–1036.
62. Herlemann DPR, et al. (2009) Genomic analysis of "*Elusimicrobium minutum*," the first cultivated representative of the phylum "*Elusimicrobia*" (formerly termite group 1). *Appl Environ Microbiol* 75(9):2841–2849.
63. Ragsdale SW, Pierce E (2008) Acetogenesis and the Wood–Ljungdahl pathway of CO_2 fixation. *Biochim Biophys Acta* 1784(12):1873–1898.
64. Thauer RK, Kaster A-K, Seedorf H, Buckel W, Hedderich R (2008) Methanogenic archaea: Ecologically relevant differences in energy conservation. *Nat Rev Microbiol* 6(8):579–591.
65. White RH (1997) Purine biosynthesis in the domain Archaea without folates or modified folates. *J Bacteriol* 179(10):3374–3377.
66. Fricke WF, et al. (2006) The genome sequence of *Methanosphaera stadtmanae* reveals why this human intestinal archaeon is restricted to methanol and H_2 for methane formation and ATP synthesis. *J Bacteriol* 188(2):642–658.
67. Sakai S, et al. (2011) Genome sequence of a mesophilic hydrogenotrophic methanogen *Methanocella paludicola*, the first cultivated representative of the order Methanocellales. *PLoS ONE* 6(7):e22898.
68. Maeder DL, et al. (2006) The *Methanosarcina barkeri* genome: Comparative analysis with *Methanosarcina acetivorans* and *Methanosarcina mazei* reveals extensive rearrangement within Methanosarcinal genomes. *J Bacteriol* 188(22):7922–7931.
69. Allen MA, et al. (2009) The genome sequence of the psychrophilic archaeon, *Methanococcoides burtonii*: The role of genome evolution in cold adaptation. *ISME J* 3(9):1012–1035.
70. Michaelis W, et al. (2002) Microbial reefs in the Black sea fueled by anaerobic oxidation of methane. *Science* 297(5583):1013–1015.
71. Milucka J, et al. (2012) Zero-valent sulphur is a key intermediate in marine methane oxidation. *Nature* 491(7425):541–546.
72. Reichard P (1993) From RNA to DNA, why so many ribonucleotide reductases? *Science* 260(5115):1773–1777.
73. Stubbe J (2000) Ribonucleotide reductases: The link between an RNA and a DNA world? *Curr Opin Struct Biol* 10(6):731–736.
74. Van Duyne GD, Standaert RF, Karplus PA, Schreiber SL, Clardy J (1993) Atomic structures of the human immunophilin FKBP-12 complexes with FK506 and rapamycin. *J Mol Biol* 229(1):105–124.
75. Fish W (1988) Rapid colorimetric micromethod for the quantitation of complexed iron in biological samples. *Methods Enzymol* 158:357.
76. Malmström BG, Reinhammar B, Vänngård T (1970) The state of copper in stellacyanin and laccase from the lacquer tree *Rhus vernicifera*. *Biochim Biophys Acta* 205(1):48–57.
77. Steeper J, Steuart C (1970) A rapid assay for CDP reductase activity in mammalian cell extracts. *Anal Biochem* 34(1):123–130.
78. Otwinowski Z, Minor W (1997) Processing of X-ray diffraction data collected in oscillation mode. *Methods Enzymology*, ed Charles W. Carter, Jr. (Academic Press, New York), Vol 276, pp 307–326.
79. Pape T, Schneider TR (2004) HKL2MAP: A graphical user interface for macromolecular phasing with SHELX programs. *J Appl Cryst* 37(5):843–844.
80. Adams PD, et al. (2010) PHENIX: A comprehensive Python-based system for macromolecular structure solution. *Acta Crystallogr D Biol Crystallogr* 66(Pt 2):213–221.
81. Emsley P, Lohkamp B, Scott WG, Cowtan K (2010) Features and development of Coot. *Acta Crystallogr D Biol Crystallogr* 66(Pt 4):486–501.
82. Tamura K, et al. (2011) MEGA5: Molecular evolutionary genetics analysis using maximum likelihood, evolutionary distance, and maximum parsimony methods. *Mol Biol Evol* 28(10):2731–2739.
83. Saitou N, Nei M (1987) The neighbor-joining method: A new method for reconstructing phylogenetic trees. *Mol Biol Evol* 4(4):406–425.
84. Jones DT, Taylor WR, Thornton JM (1992) The rapid generation of mutation data matrices from protein sequences. *Comput Appl Biosci* 8(3):275–282.
85. Eyre-Walker A, Keightley PD (2007) The distribution of fitness effects of new mutations. *Nat Rev Genet* 8(8):610–618.
86. Felsenstein J (1978) Cases in which parsimony or compatibility methods will be positively misleading. *Syst Biol* 27(4):401–410.
87. Letunic I, Bork P (2007) Interactive Tree Of Life (iTOL): An online tool for phylogenetic tree display and annotation. *Bioinformatics* 23(1):127–128.